Kegl, M., Brank, B. 2006. Shape optimization of truss-stiffened shell structures with variable thickness. *Comput. methods appl. mech. eng.*, 195, 19/22: 2611-2634.

http://dx.doi.org/10.1016/j.cma.2005.05.020

SHAPE OPTIMIZATION OF TRUSS-STIFFENED SHELL STRUCTURES WITH VARIABLE THICKNESS

M. KEGL

Faculty of Mechanical Engineering, University of Maribor, Smetanova 17, 2000 Maribor, Slovenia

B. BRANK

Faculty of Civil and Geodetic Engineering, University of Ljubljana, Jamova 2, 1000 Ljubljana, Slovenia

ADDRESS:

M. Kegl
FACULTY OF MECHANICAL ENGINEERING
Smetanova 17
SI-2000 Maribor
Slovenia

Telephone: (+386 2) 220-7802
Fax: (+386 2) 220-7990
E-mail: marko.kegl@uni-mb.si

SHAPE OPTIMIZATION OF TRUSS-STIFFENED SHELL STRUCTURES WITH VARIABLE THICKNESS

M. KEGL

Faculty of Mechanical Engineering, University of Maribor, Smetanova 17, 2000 Maribor, Slovenia

B. BRANK

Faculty of Civil and Geodetic Engineering, University of Ljubljana, Jamova 2, 1000 Ljubljana, Slovenia

ABSTRACT

This paper presents an effective approach to shape optimal design of statically loaded elastic shell-like structures. The shape parametrization is based on a design element technique. The chosen design element is a rational Bézier body, enhanced with a smoothly varying scalar field. A body-like design element makes possible to unify the shape optimization of both pure shells and truss-stiffened shell structures. The scalar field of the design element is obtained by attaching to each control point a scalar quantity, which is an add-on to the position and weight of the control point. This scalar field is linked to the shell thickness distribution, which can be optimized simultaneously with the shape of the shell. For linear and non-linear analysis of shell structures, a reliable 4-node shell finite element formulation is utilized. The presented optimization approach assumes the employment of a gradient-based optimization algorithm and the use of the discrete method of direct differentiation to perform the sensitivity analysis. Four numerical examples of shell and truss-stiffened shell optimization are presented in detail to illustrate the performance of the proposed approach.

KEYWORDS: shape, optimization, truss-stiffened shell, design element, Bézier body

1. INTRODUCTION

In order to find effective shapes of shell-like structures many ideas have been investigated and proposed. They may be roughly summarized into three main streams: the principle of a hanging model, the soap film analogy, and structural optimization. The approaches of the first two groups primarily use experimental tests, although they may also use numerical simulations (see e.g. references in [5]). The approaches based on structural optimization, however, are probably the most general and the most promising ones.

During the last several years different techniques for shape optimal design of shells, which can be classified under structural optimization, have been proposed. Maute and Ramm [22] combined shape optimization (in order to get smooth contours of the shell) with material topology optimization (in order to get the basic layout). Ansola et al. [2] presented an integrated approach to shape and topology optimization of shells in order to minimize the compliance of the structure. Lindbay and Santos [21] focused their work on shape optimization of shells by employing the shape parametrization of an existing CAD system (the aim was to take full advantage of geometric modeling and automatic meshing capabilities of the CAD system). Ohsaki et al. [25] proposed to seek for optimal shapes taking into account the fairness metrics of curves and surfaces, optionally in combination with mechanical quantities such as compliance. Lagaros et al. [19] addressed the evolution strategy based discrete optimization of single-layered shells with stiffening beams: the design variables were related to some shape parameters of the structure as well as to the sizing parameters and topology of the stiffeners. Gates and Accorsi [11] performed shape optimization by successively selecting the most appropriate edge of the shell and moving it by employing non-linear optimization combined with a commercial analysis code. Imam [13] presented an approach to shape optimization of umbrella-shaped concrete shells. For further interesting discussions and examples related to the optimal shape design of shells the reader may also refer to [1,4,6,9,12,17,20,26,27].

It seems that the above mentioned paper of Lagaros et al. is one of the few works addressing optimization of shell structures with stiffeners. To the authors' knowledge there are no papers addressing shape optimization of truss-stiffened shells with variable thickness. This makes the present work different from the related published works.

The shape optimization approach proposed in this paper is based on a design element technique. As a design element a rational Bézier body is chosen. The shell middle surface is assumed to occupy a particular parametric surface of the design element, while the rest of the element may be occupied by an arbitrary truss structure. By the shape variation of the design element the shapes of the shell part and the truss part of the structure are varied simultaneously and consistently.

The thickness of the shell may also be variable. This is achieved by enhancing the design element with a smooth scalar field and by further linking it with the shell thickness. The scalar field is introduced by attaching an additional scalar quantity (called *value* of the control point) to each control point of the Bézier body and by employing the interpolation functions of the design element. A similar idea was also used by Ohsaki et al. [24], where the cross-sectional areas of truss elements were linked to Bézier curves.

By adopting the above approach, the shape of variable thickness shell structures with or without truss stiffeners can be optimized in a unified and relatively simple way. The stiffening truss

structure may be of any kind including double and multi-layered trusses, and may lie on one or both sides of the shell. The design variables may be related to the *positions*, *weights* and *values* of the design element control points as well as to the cross-sections of truss finite elements. The optimization is assumed to be performed by a gradient-based optimization algorithm and the sensitivity analysis is done by the discrete approach of direct differentiation.

The outline of the paper is as follows. Section 2 briefly presents the finite elements used and their geometrical data varied during the shape optimization. Section 3 presents the shape parameterization concept and the enhanced design element. In Section 4 the optimal design problem is formulated and its solution procedure is discussed briefly. Finally, Section 5 presents four numerical examples in full detail.

2. FINITE ELEMENTS USED IN OPTIMIZATION PROCESS

Non-linear truss and non-linear shell finite elements that may undergo large displacements and large rotations (but small strains) are used in the optimization process. The truss element is a standard 2-node element with a constant cross-section. Its internal force vector $\mathbf{F}^e$, the loading vector $\mathbf{R}^e$, and the tangential stiffness matrix $\mathbf{K}^e$ can be derived in closed forms. From the geometrical point of view, the element is fully specified by position of its nodes $\mathbf{r}_n$, $n = 1,2$, and the area of cross-section A (see Figure 1a).

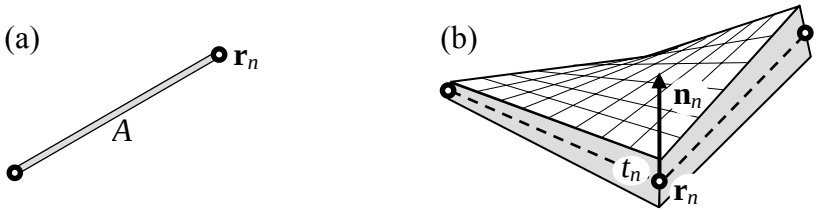

Figure 1. Geometrical quantities of truss and shell finite element

The 4-node shell finite element is based on an ANS (assumed natural strain) concept of Bathe and Dvorkin [3]; see also [8], [30]. Finite rotations are parametrized by a constrained rotation vector, e.g. [7], which is consistent with the standard incremental solution scheme for non-linear problems. Since it maintains additive iterative rotational updates it is also very suitable for optimization problems [12]. The usual 4-node ANS shell element formulation is modified to suit the analysis of shells with variable thickness. According to the isoparametric concept, the position vector of a shell middle surface point $\mathbf{r}$, the normal vector to the middle surface $\mathbf{n}$ and the shell thickness t are given (for the undeformed configuration) as

$$\mathbf{r} = \sum_{n=1}^{4} N_n \mathbf{r}_n, \qquad \mathbf{n} = \sum_{n=1}^{4} N_n \mathbf{n}_n, \qquad t = \sum_{n=1}^{4} N_n t_n \tag{1}$$

where

$$N_n = \frac{1}{4}(1+\xi\,\xi_n)(1+\eta\eta_n), \qquad n = 1,\ldots,4 \tag{2}$$

are usual bi-linear interpolation functions, and $(\xi_n, \eta_n) \in \{(-1,-1),(1,-1),(1,1),(-1,1)\}$. The geometry of the element is fully specified by Eqs. (1)-(2), and by the position of its nodes $\mathbf{r}_n$, nodal normals $\mathbf{n}_n$ and nodal thicknesses $t_n, n = 1,2,3,4$ (see Figure 1b). These quantities are needed for computation of the internal force vector $\mathbf{F}^e$, the loading vector $\mathbf{R}^e$ and the tangential stiffness matrix $\mathbf{K}^e$ of the element, which should be remembered when performing the sensitivity analysis.

In this work it is assumed that cross-section A of the truss element is linked to the design variables in a usual way (as in conventional sizing optimization). On the other hand, nodal positions of both truss and shell elements $\mathbf{r}_n$, nodal normals $\mathbf{n}_n$, and nodal thicknesses t_n of the shell element, are all linked to the design variables via the design element.

The internal and the external force vectors

$$\mathbf{F}^e = \left[\mathbf{F}_1^e, \mathbf{F}_2^e, \mathbf{F}_3^e, \mathbf{F}_4^e\right]^T, \quad \mathbf{R}^e = \left[\mathbf{R}_1^e, \mathbf{R}_2^e, \mathbf{R}_3^e, \mathbf{R}_4^e\right]^T \tag{3}$$

of the non-linear shell finite element can be written as (see e.g. [8], [30])

$$\begin{aligned} \mathbf{F}_n^e &= \int_{\Omega^e} \left\{ \sum_{l=1}^{4} \left[\left(\widetilde{\mathbf{B}}_n^m\right)^T \mathbf{C}^m \widetilde{\mathbf{B}}_l^m + \left(\widetilde{\mathbf{B}}_n^b\right)^T \mathbf{C}^b \widetilde{\mathbf{B}}_l^b + \left(\widetilde{\mathbf{B}}_n^s\right)^T \mathbf{C}^s \widetilde{\mathbf{B}}_l^s \right] \mathbf{u}_l \right\} \widetilde{j}\, d\xi\, d\eta \\ \mathbf{R}_n^e &= \int_{\Omega^e} \widetilde{\mathbf{P}}_n \, \widetilde{j}\, d\xi\, d\eta \end{aligned} \tag{4}$$

The matrices $\widetilde{\mathbf{B}}_i^m, \widetilde{\mathbf{B}}_i^b, \widetilde{\mathbf{B}}_i^s$ are obtained from variation (linearization) of membrane, bending and transverse shear strains, respectively, while the matrices $\mathbf{C}^m, \mathbf{C}^b, \mathbf{C}^s$ define the linear elastic constitutive relations for shells. Vector $\widetilde{\mathbf{P}}_n$ collects shell area loading, which is in this paper assumed as conservative, $\widetilde{j} = \left| \frac{\partial \mathbf{r}}{\partial \xi} \times \frac{\partial \mathbf{r}}{\partial \eta} \right|$ is the Jacobian of the isoparametric transformation from the undeformed finite element space to the bi-unit square $\Omega^e = [-1,1] \times [-1,1]$, and $\mathbf{u}_l$ is a vector of displacements/rotations at node *l*. Note that the $\widetilde{\mathbf{B}}$ matrices, $\widetilde{\mathbf{P}}_n$ and $\widetilde{j}$ are functions of position vector $\mathbf{r}$, and that the $\widetilde{\mathbf{B}}$ and $\mathbf{C}$ matrices are functions of thickness t. Vector $\widetilde{\mathbf{P}}_n$ also depends on t if self-weight is taken into account.

3. SHAPE PARAMETRIZATION BY USING AN ENHANCED DESIGN ELEMENT

3.1 Design element

In order to parametrize the shape of the structure, the design element technique is employed with a rational Bézier body as a chosen design element (DE). The Bézier body exhibits good shape flexibility, automatic prevention of excessive shape oscillations and possible representation of classical shapes. A body-like DE is preferred over a surface-like DE in order to unify shape optimization of both shell structures (i.e. surface-like structures) and truss-stiffened shell structures (i.e. body-like structures) (see Figure 2).

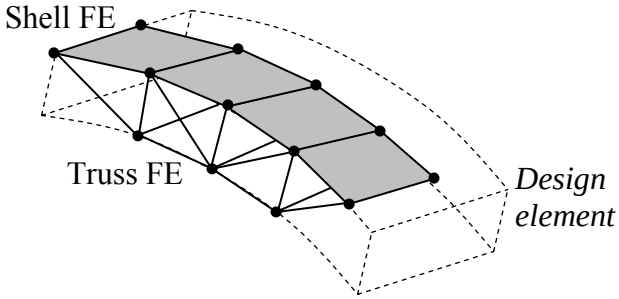

Figure 2. A body-like design element

The Bézier body is defined by a topologically rectangular scheme of $N_1 \times N_2 \times N_3$ *control points* P_{ijk}. Conventionally, the attributes of each control point P_{ijk} are its *position* $\mathbf{q}_{ijk}$ and the corresponding *weight* w_{ijk}. In this work, however, an additional scalar quantity h_{ijk}, called the *value* of the control point P_{ijk}, is attached to each control point (see Figure 3). By adopting such an arrangement, the shape of the Bézier body is still defined in the conventional way (by the control point positions and by weights). The above mentioned values of the control points are used to introduce a smooth scalar field, defined over the whole Bézier body, which can be linked for example to the shell thickness.

The DE shape depends on the *design variables* - a set of independent parameters $b_1, b_2, \ldots, b_N$ assembled in vector $\mathbf{b} \in \mathrm{R}^N$. This is achieved by assuming that $\mathbf{q}_{ijk}$, w_{ijk} and h_{ijk} are not necessarily constants, but may depend on $\mathbf{b}$. Thus, one has $\mathbf{q}_{ijk} = \mathbf{q}_{ijk}(\mathbf{b})$, $w_{ijk} = w_{ijk}(\mathbf{b})$, and $h_{ijk} = h_{ijk}(\mathbf{b})$.

Remark. In a general purpose code, there are several possibilities for implementing these dependencies. In this work an arithmetic expression parser is integrated into the code. In this way any component of $\mathbf{q}_{ijk}$, w_{ijk} or h_{ijk} may be defined by an arithmetic expression in terms of $b_1, b_2, \ldots, b_N$ by using the FORTRAN syntax. The same parser is also responsible for the calculation

of the design derivatives of these quantities. Thus, one has a possibility to conveniently define design dependent quantities $\mathbf{q}_{ijk}$, w_{ijk}, h_{ijk} and to easily compute the design derivatives $d\mathbf{q}_{ijk}/d\mathbf{b}$, $dw_{ijk}/d\mathbf{b}$ and $dh_{ijk}/d\mathbf{b}$ needed in the sensitivity analysis.

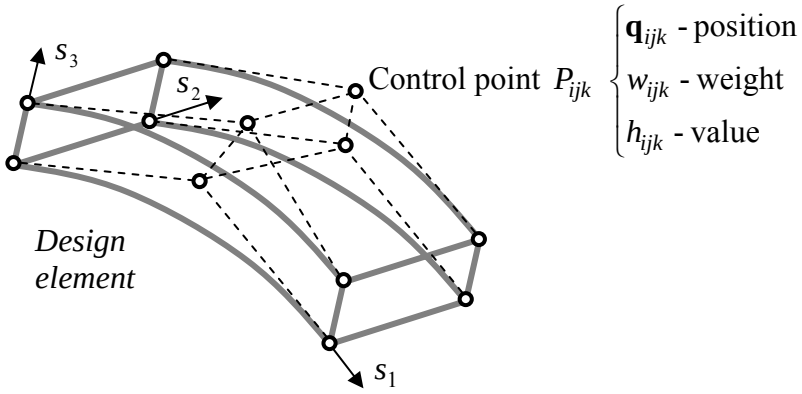

Figure 3. Control point P_{ijk}, its position $\mathbf{q}_{ijk}$, weight w_{ijk} and value h_{ijk}

A Bézier body has a local curvilinear coordinate system with its coordinates s_1, s_2 and s_3 running from 0 to 1 (see Figure 3). Thus, vector $\mathbf{s} = [s_1 \quad s_2 \quad s_3]^T$ defines a point in the DE coordinate system. For any point $\mathbf{s}$ there is an image $\mathbf{r}$ in the real 3-D space

$$\mathbf{r} = \mathbf{r}(\mathbf{s}, \mathbf{b}) = \frac{\sum_{i=1}^{N_1}\sum_{j=1}^{N_2}\sum_{k=1}^{N_3} B_i^{N_1} B_j^{N_2} B_k^{N_3} w_{ijk} \mathbf{q}_{ijk}}{\sum_{i=1}^{N_1}\sum_{j=1}^{N_2}\sum_{k=1}^{N_3} B_i^{N_1} B_j^{N_2} B_k^{N_3} w_{ijk}} \tag{5}$$

and a corresponding scalar quantity t

$$t = t(\mathbf{s}, \mathbf{b}) = \frac{\sum_{i=1}^{N_1}\sum_{j=1}^{N_2}\sum_{k=1}^{N_3} B_i^{N_1} B_j^{N_2} B_k^{N_3} w_{ijk} h_{ijk}}{\sum_{i=1}^{N_1}\sum_{j=1}^{N_2}\sum_{k=1}^{N_3} B_i^{N_1} B_j^{N_2} B_k^{N_3} w_{ijk}} \tag{6}$$

where $B_i^{N_1} = B_i^{N_1}(s_1)$, $B_j^{N_2} = B_j^{N_2}(s_2)$ and $B_k^{N_3} = B_k^{N_3}(s_3)$ are the Bernstein´s blending polynomials of the orders of $N_1 - 1$, $N_2 - 1$ and $N_3 - 1$, respectively, [10].

3.2 Finite element attachment to the design element

When using body-like DE for parametrization of a shell structure, it is convenient that the shell middle surface coincides with some parametric surface of the DE. Without loss of generality, it is assumed in what follows that the shell middle surface is defined as $s_3 = s_{3c}$ surface of the DE,

where s_{3c} is any fixed value between 0 and 1. It follows from Eq. (5) that a point on the shell middle surface can be expressed as $\mathbf{r}=\mathbf{r}(\mathbf{s}_c,\mathbf{b})$, where $\mathbf{s}_c=[s_1 \quad s_2 \quad s_{3c}]^T$. By using Eq. (6), a smoothly varying thickness of the shell is given as $t=t(\mathbf{s}_c,\mathbf{b})$. And the shell director vector field $\mathbf{n}$, being normal to the middle surface, is given as

$$\mathbf{n}=\mathbf{n}(\mathbf{s}_c,\mathbf{b})=\left[\frac{\partial\mathbf{r}(\mathbf{s}_c,\mathbf{b})}{\partial s_1}\times\frac{\partial\mathbf{r}(\mathbf{s}_c,\mathbf{b})}{\partial s_2}\right]\Bigg/\left|\frac{\partial\mathbf{r}(\mathbf{s}_c,\mathbf{b})}{\partial s_1}\times\frac{\partial\mathbf{r}(\mathbf{s}_c,\mathbf{b})}{\partial s_2}\right| \tag{7}$$

By the proposed design element technique, the position of a particular finite element node is fully specified by its position $\mathbf{s}$ in the parametric space (see [16]). Once the position $\mathbf{s}$ of the shell finite element (SFE) node is known, Eq. (5) is used to calculate its position $\mathbf{r}$ in the real 3-D space *for any* given values of the design variables $\mathbf{b}$. By using Eq. (6) the thickness of the shell at the node under consideration can be calculated, while Eq. (7) is used to calculate the corresponding nodal shell director.

Assuming that the DE data $\mathbf{q}_{ijk}$, w_{ijk} and h_{ijk} are known, all the geometrical data for the SFE can be obtained from the parametric positions of its nodes. In other words, the geometrical data for the SFE are fully specified by four points $\{\mathbf{s}_{cn}, n=1,2,3,4\}$. These points can be regarded as the pre-images of the SFE nodal positions in the real 3-D space. The middle surface position $\mathbf{r}$, the thickness t and the normal $\mathbf{n}$ at any point of the SFE can now be derived as shown in Figure 4.

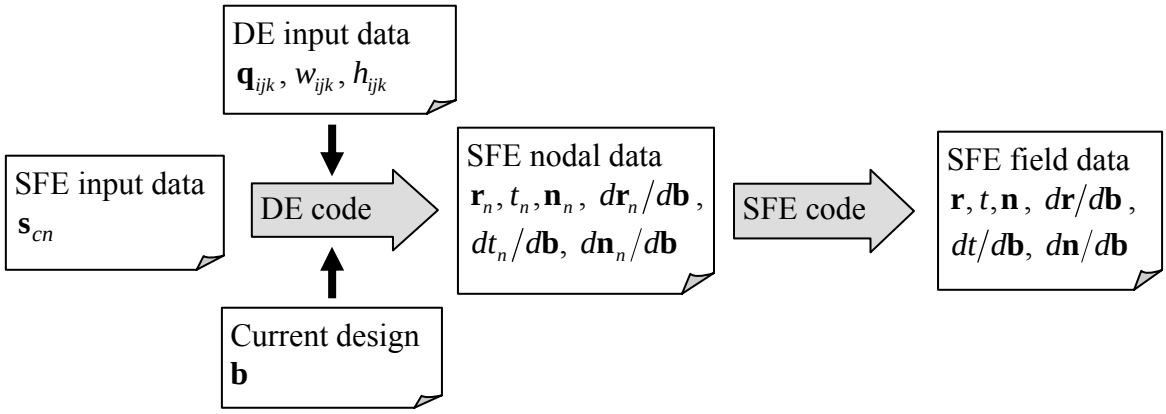

Figure 4. Geometrical data retrieval for the SFE

It should be noted that the DE is used only to obtain the nodal geometrical data $\mathbf{r}_n=\mathbf{r}(\mathbf{s}_{cn},\mathbf{b})$, $t_n=t(\mathbf{s}_{cn},\mathbf{b})$, $\mathbf{n}_n=\mathbf{n}(\mathbf{s}_{cn},\mathbf{b})$ of the SFE and the corresponding design derivatives

$$\frac{d\mathbf{r}_n}{d\mathbf{b}}=\frac{d\mathbf{r}(\mathbf{s}_{cn},\mathbf{b})}{d\mathbf{b}},\quad \frac{dt_n}{d\mathbf{b}}=\frac{dt(\mathbf{s}_{cn},\mathbf{b})}{d\mathbf{b}},\quad \frac{d\mathbf{n}_n}{d\mathbf{b}}=\frac{d\mathbf{n}(\mathbf{s}_{cn},\mathbf{b})}{d\mathbf{b}} \tag{8}$$

needed for the sensitivity analysis. Once the nodal data are known, the geometrical field data, needed for the integration over the element, are obtained by employing the SFE shape functions.

Thus, the SFE middle surface, the director and the thickness are given by Eqs. (1) while the derivatives of the same quantities with respect to **b** are

$$\frac{d\mathbf{r}}{d\mathbf{b}} = \sum_{n=1}^{4} N_n \frac{d\mathbf{r}_n}{d\mathbf{b}}, \qquad \frac{dt}{d\mathbf{b}} = \sum_{n=1}^{4} N_n \frac{dt_n}{d\mathbf{b}}, \qquad \frac{d\mathbf{n}}{d\mathbf{b}} = \sum_{n=1}^{4} N_n \frac{d\mathbf{n}_n}{d\mathbf{b}} \tag{9}$$

Note that by adopting the above procedure the shape of the shell (and the corresponding finite element mesh) is actually parametrized in terms of the design variables $\mathbf{b}$.

If the shell is stiffened by a truss structure, a consistent shape variation of both the shell and the truss structure has to be assured. For this purpose the truss elements should also be mapped to the real 3-D space from the DE domain. In other words, the position of a truss finite element should also be specified by two points $\{\mathbf{s}_n, n = 1,2\}$. Of course, the parametric coordinate s_3 of the node may now have any value between 0 and 1, meaning that the truss finite element may me positioned anywhere within the DE. The actual nodal positions $\mathbf{r}_n, n = 1,2$ of the truss element and the corresponding design derivatives $d\mathbf{r}_n / d\mathbf{b}, n = 1,2$ are obtained in the same manner as for the shell element.

3.3 Combining design elements

To model a structure, one or more design elements can be used. When several design elements are utilized, some considerations, related to the continuity along the common boundary of two adjacent design elements, are needed. Positional or C^0 continuity is required practically always; on the other hand, also slope or C^1 continuity is often a desired feature.

Generally, the positional and slope continuity may be relatively easily obtained only in certain situations. Let the symbols α and β denote two adjacent design elements that need to have a common boundary surface. Since α and β are Bézier bodies, their boundary surfaces consist of 6 Bézier patches and the 4 boundary curves of each of these patches are Bézier curves [10]. In order to obtain continuity in a relatively simple manner, it is required that a boundary patch as a whole is shared by both design elements α and β. Thus, it should be avoided to trying to match a boundary patch of α with only a part of a boundary patch of β. An exception to this guideline is a situation where one of the design elements is degenerated to a surface. In this case one whole boundary (edge) curve should be shared by α and β. Again, it should be avoided to trying to match one boundary curve of α with some arbitrary parametric curve on the surface of β.

Taking into account the above restrictions, positional continuity can be obtained in a very simple way. The only requirement is that the matching boundary patches share the same set of control points. Of course, this also means that the number of control points in both directions of the

matching patches has to be the same, i.e. the patches must match topologically.

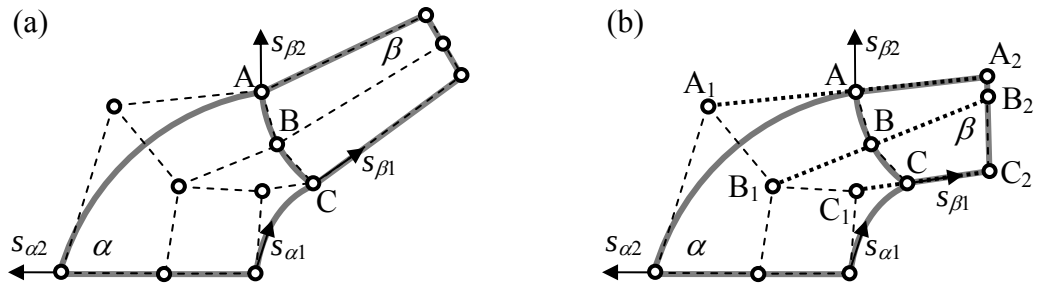

Figure 5. Continuity on topologically matching boundary patches

Figure 5a illustrates a situation where a $3\times3\times1$ design element α is combined with a $2\times3\times1$ design element β. Positional continuity is obtained by the control points A, B and C which are the same for the common boundary curve. In a more general situation, let α and β be two adjacent design elements with $N_{\alpha1}\times N_{\alpha2}\times N_{\alpha3}$ and $N_{\beta1}\times N_{\beta2}\times N_{\beta3}$ control points, respectively. Let the desired common patch be, for example, the $s_1^\alpha = 1$ boundary patch of α and the $s_1^\beta = 0$ boundary patch of β. The symbols s_i^α and s_i^β are used to denote the local coordinates of the design elements α and β. In order to achieve positional continuity in a relative simple manner, one should define

$$\begin{aligned} &N_{\alpha2} \equiv N_{\beta2}, \quad N_{\alpha3} \equiv N_{\beta3} \\ &\mathbf{q}^\alpha_{N_{\alpha1}jk} \equiv \mathbf{q}^\beta_{1jk}, \quad h^\alpha_{N_{\alpha1}jk} \equiv h^\beta_{1jk}, \quad 1 \le j \le N_{\alpha2}, \quad 1 \le k \le N_{\alpha3} \end{aligned} \tag{10}$$

Similarly, positional continuity requirements may be obtained for any possible combination of boundary patches of α and β.

For slope continuity, additional constraints on control point positions have to be introduced. These constraints require that each common control point lies on a straight line, defined by its both neighboring control points (in the parametric direction that crosses the design element boundaries). In the example situation discussed above, the additional constraints assuring slope continuity can be written as follows

$$\begin{aligned} &\mathbf{q}^\alpha_{N_{\alpha1}jk} = \xi\mathbf{q}^\alpha_{N_{\alpha1}-1jk} + (1-\xi)\mathbf{q}^\beta_{2jk}, \\ &h^\alpha_{N_{\alpha1}jk} = \xi h^\alpha_{N_{\alpha1}-1jk} + (1-\xi)h^\beta_{2jk}, \quad 1 \le j \le N_{\alpha2}, \quad 1 \le k \le N_{\alpha3} \end{aligned} \tag{11}$$

where ξ is an arbitrary value chosen so that $0 < \xi < 1$. Figure 5b illustrates a situation where positional and slope continuity is assured by proper positioning of adequate control points. The common control points A, B and C lie on the straight (dotted) lines defined by the neighboring control points A_1 through C_2.

It should be noted that the above constraints for positional and slope continuity can simply be introduced implicitly by an adequate definition of the design elements and control points. Thus, for positional continuity the adjacent design elements only need to share the same set of control points that define the common patch. For slope continuity, these common control points need to be expressed in terms of their neighbors. Additional explicit constraints that would increase the size of the problem are therefore not needed.

In certain situations it may be of benefit to combine two design elements whose adjacent patches do not match topologically (see Figure 6). In general, assuring slope continuity in such a case is rather cumbersome. However, positional continuity might be obtained relatively easily, if the common patch is (and also remains during the optimization) a quadrilateral, i.e. a plane surface with straight edges. In addition, the control points on the common surface have to be distributed uniformly (see Figure 6a) in order to assure that the FE mesh in both design elements may be matched easily on the common surface (see Figure 6b).

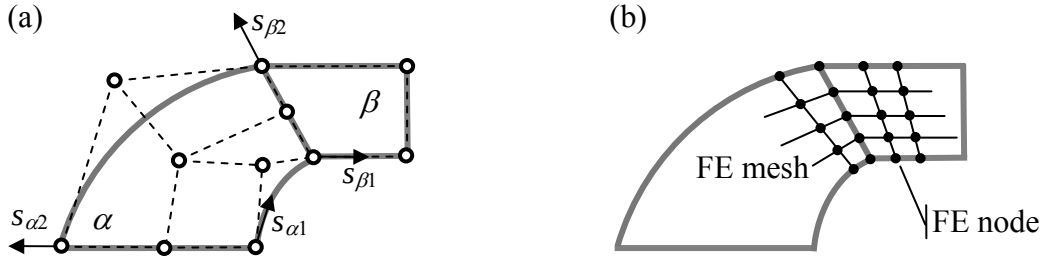

Figure 6. Positional continuity on topologically mismatching boundary patches

Quadrilateral boundary patch and uniform distribution can be achieved simply by defining all the involved control points in terms of the 4 corner control points. In the example situation discussed above, this can be expressed as

$$\begin{aligned}
\mathbf{q}^{\alpha}_{N_{\alpha 1} jk} = \frac{1}{4}\Big[&(1-\eta_j)(1-\zeta_k)\mathbf{q}^{\alpha}_{N_{\alpha 1}11} + (1+\eta_j)(1-\zeta_k)\mathbf{q}^{\alpha}_{N_{\alpha 1}N_{\alpha 2}1} + \\
&(1+\eta_j)(1+\zeta_k)\mathbf{q}^{\alpha}_{N_{\alpha 1}N_{\alpha 2}N_{\alpha 3}} + (1-\eta_j)(1+\zeta_k)\mathbf{q}^{\alpha}_{N_{\alpha 1}1N_{\alpha 3}}\Big] \\
h^{\alpha}_{N_{\alpha 1} jk} = \frac{1}{4}\Big[&(1-\eta_j)(1-\zeta_k)h^{\alpha}_{N_{\alpha 1}11} + (1+\eta_j)(1-\zeta_k)h^{\alpha}_{N_{\alpha 1}N_{\alpha 2}1} + \\
&(1+\eta_j)(1+\zeta_k)h^{\alpha}_{N_{\alpha 1}N_{\alpha 2}N_{\alpha 3}} + (1-\eta_j)(1+\zeta_k)h^{\alpha}_{N_{\alpha 1}1N_{\alpha 3}}\Big]
\end{aligned} \tag{12}$$

where

$$\eta_j = \frac{2(j-1)}{N_{\alpha 2}-1} - 1, \quad \zeta_k = \frac{2(k-1)}{N_{\alpha 3}-1} - 1, \quad 1 \le j \le N_{\alpha 2}, \quad 1 \le k \le N_{\alpha 3} \tag{13}$$

Similar relations have to be used if some other combination of boundary patches needs to be matched. Figure 7a illustrates a situation where positional continuity is assured on a common patch

between the $N_{\alpha 1} \times 2 \times 2$ design element α and the $N_{\beta 1} \times 3 \times 3$ design element β.

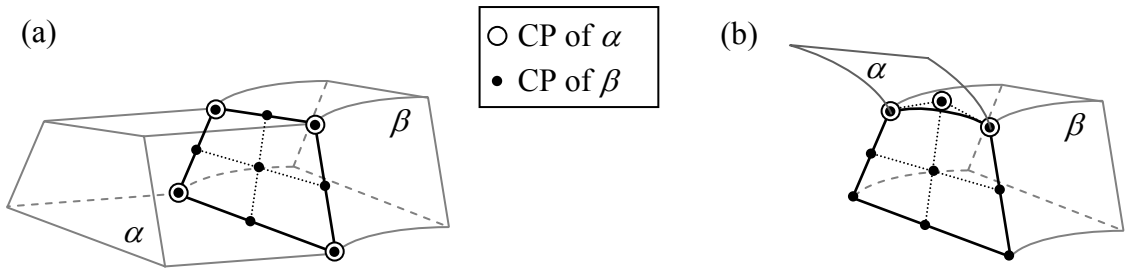

Figure 7. Positional continuity for body-body and surface-body situation

Finally, Figure 7b illustrates a situation where a boundary curve of a degenerated (surface-like) design element is combined with a boundary (edge) curve of a body-like design element. In such cases positional continuity can easily be obtained by using the same control points for the matching curves. In addition, if the matching curves also match topologically, slope continuity can be obtained easily by following the guidelines already discussed for the body-body situation.

4. FORMULATION AND SOLUTION OF THE OPTIMAL DESIGN PROBLEM

An optimization problem of a statically loaded structure can usually be written in the following form

$$\min f_0 \tag{14}$$

subject to constraints

$$\begin{aligned} f_i &\le 0, \quad i = 1, \ldots, M \\ b_i^L &\le b_i \le b_i^U, \quad i = 1, \ldots, N \end{aligned} \tag{15}$$

Here $f_0 = f_0(\mathbf{b}, \mathbf{u})$ denotes the objective function, which is often defined as the volume, compliance, or strain energy of the structure. The constrained quantities $f_i = f_i(\mathbf{b}, \mathbf{u})$ are usually nodal displacements and rotations, element strains and stresses, geometrical constraints and technological limitations. The symbols b_i^L and b_i^U denote the lower and the upper limits of the design variables, while $\mathbf{u}$ is a vector of structural response variables – usually nodal displacements and rotations.

It should be emphasized that in problem (14)-(15) the design variables shall be considered as independent and the response variables as dependent variables. In other words, the dependency $\mathbf{u} = \mathbf{u}(\mathbf{b})$ is established implicitly by the structural equilibrium equation

$$\mathbf{F} - \mathbf{R} = \mathbf{0} \tag{16}$$

where $\mathbf{F}$ and $\mathbf{R}$ denote the vectors of structural internal and external forces.

Structural vectors $\mathbf{F}$ and $\mathbf{R}$ are obtained by assembling individual finite element vectors $\mathbf{F}^e$ and $\mathbf{R}^e$. For the shell finite element these vectors are obtained from Eqs. (4), where the geometrical data, corresponding to the current design, have to be computed in accordance with the scheme shown in Figure 4. The geometrical data needed for the computation of internal forces and loads in the truss element are obtained in the same manner.

Since the design variables $\mathbf{b}$ are continuous, a gradient-based optimization algorithm can be used to solve the problem (14)-(15). In this case the solution procedure is iterative and can be outlined as follows:

Solution procedure

1. Set $k = 0$; choose some initial $\mathbf{b}^{(0)}$.
2. Calculate $f_i, i = 0,\ldots,M$ at $\mathbf{b}^{(k)}$ (response analysis).
3. Calculate $df_i/d\mathbf{b}, i = 0,\ldots,M$ at $\mathbf{b}^{(k)}$ (sensitivity analysis).
4. Submit the calculated values to the optimizer in order to obtain some improvement $\Delta\mathbf{b}^{(k)}$ and calculate the improved design $\mathbf{b}^{(k+1)} = \mathbf{b}^{(k)} + \Delta\mathbf{b}^{(k)}$.
5. Set $k = k+1$ and check some appropriate convergence criteria – if fulfilled exit, otherwise go to Step 2.

In order to perform the response and sensitivity analysis, $\mathbf{u}^{(k)}$ and $\left(d\mathbf{u}/d\mathbf{b}\right)^{(k)}$ have to be calculated at given $\mathbf{b}^{(k)}$. The response $\mathbf{u}^{(k)}$ is obtained from the response equation (16), while $\left(d\mathbf{u}/d\mathbf{b}\right)^{(k)}$ has to be calculated from the corresponding sensitivity equation (see e.g. [29])

$$\left(\frac{\partial\mathbf{F}}{\partial\mathbf{u}} - \frac{\partial\mathbf{R}}{\partial\mathbf{u}}\right)\frac{d\mathbf{u}}{d\mathbf{b}} = \frac{\partial\mathbf{R}}{\partial\mathbf{b}} - \frac{\partial\mathbf{F}}{\partial\mathbf{b}} \tag{17}$$

Note that the term in the parentheses on the left is the tangential stiffness matrix of the structure. This matrix is known (and already decomposed) from the response analysis. Thus, the sensitivity equation can be solved with a rather small additional computational effort: only partial design derivatives of internal and external forces – the terms on the right hand side of Eq. (17) – need to be computed.

The shell finite element contributions to $\partial\mathbf{F}/\partial\mathbf{b}$ and $\partial\mathbf{R}/\partial\mathbf{b}$ can be expressed as

$$\frac{\partial\mathbf{F}^e}{\partial\mathbf{b}} = \left[\frac{\partial\mathbf{F}_1^e}{\partial\mathbf{b}}, \frac{\partial\mathbf{F}_2^e}{\partial\mathbf{b}}, \frac{\partial\mathbf{F}_3^e}{\partial\mathbf{b}}, \frac{\partial\mathbf{F}_4^e}{\partial\mathbf{b}}\right], \quad \frac{\partial\mathbf{R}^e}{\partial\mathbf{b}} = \left[\frac{\partial\mathbf{R}_1^e}{\partial\mathbf{b}}, \frac{\partial\mathbf{R}_2^e}{\partial\mathbf{b}}, \frac{\partial\mathbf{R}_3^e}{\partial\mathbf{b}}, \frac{\partial\mathbf{R}_4^e}{\partial\mathbf{b}}\right] \tag{18}$$

where

$$\frac{\partial \mathbf{F}_n^e}{\partial \mathbf{b}} = \int_{\Omega^e} \frac{\partial}{\partial \mathbf{b}} \left\{ \sum_{l=1}^{4} \left[\left(\widetilde{\mathbf{B}}_n^m\right)^T \mathbf{C}^m \widetilde{\mathbf{B}}_l^m + \left(\widetilde{\mathbf{B}}_n^b\right)^T \mathbf{C}^b \widetilde{\mathbf{B}}_l^b + \left(\widetilde{\mathbf{B}}_n^s\right)^T \mathbf{C}^s \widetilde{\mathbf{B}}_l^s \right] \mathbf{u}_l \right\} \widetilde{j}\, d\xi\, d\eta + \int_{\Omega^e} \left\{ \sum_{l=1}^{4} \left[\left(\widetilde{\mathbf{B}}_n^m\right)^T \mathbf{C}^m \widetilde{\mathbf{B}}_l^m + \left(\widetilde{\mathbf{B}}_n^b\right)^T \mathbf{C}^b \widetilde{\mathbf{B}}_l^b + \left(\widetilde{\mathbf{B}}_n^s\right)^T \mathbf{C}^s \widetilde{\mathbf{B}}_l^s \right] \mathbf{u}_l \right\} \frac{\partial \widetilde{j}}{\partial \mathbf{b}}\, d\xi\, d\eta \qquad (19)$$

$$\frac{\partial \mathbf{R}_n^e}{\partial \mathbf{b}} = \int_{\Omega^e} \left(\frac{\partial \widetilde{\mathbf{P}}_n}{\partial \mathbf{b}} \widetilde{j} + \widetilde{\mathbf{P}}_n \frac{\partial \widetilde{j}}{\partial \mathbf{b}} \right) d\xi\, d\eta$$

Note that the design derivatives in Eqs. (19) turn out to be very complicated expressions. In this work they are obtained by using a system for symbolic derivation and automatic code generation [18]. The derivation of the corresponding expressions for the truss element is straightforward. All the geometrical quantities and their design derivatives, needed for this computation, have to be obtained in accordance with the scheme shown in Figure 4.

The above outlined solution procedure of the optimization problem can be implemented in several different ways. In this work a separate (stand-alone) optimization program and a separate analysis program (see Figure 8) have been used. This arrangement enables multi-case optimizations (the same simulator is run several times) as well as the solution of complex optimization problems (several different simulators are run as necessary). In any case the optimizer runs all the simulations, acquires all their output data, assembles the data into a single optimization problem and makes use of its own built-in optimization algorithm to improve the design. This procedure is repeated in each cycle of the optimization process.

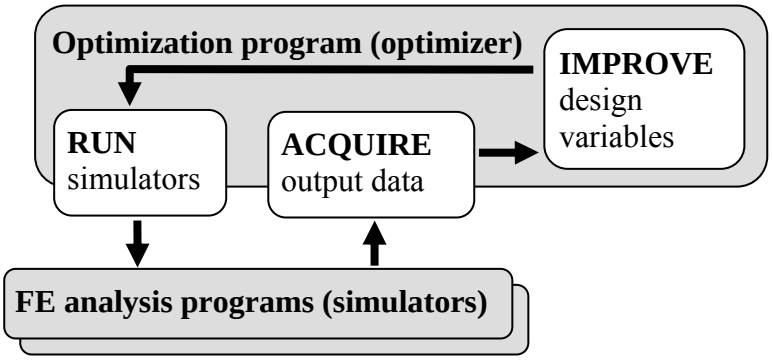

Figure 8. Implementation of the solution procedure

The whole process is driven by the optimizer which controls the execution of simulation processes and the data exchange. The data exchange between separately running programs is established by XML conforming data files. That means that the simulator can be any program meeting some minimal data exchange requirements related to the format of the input and output files.

5. NUMERICAL EXAMPLES

In order to illustrate the approach presented above, four numerical examples are considered. The first one (a pressure vessel strip) is seen as a correctness test of the approach. The second one illustrates the shape optimization of a shell structure with variable thickness. The third example demonstrates the optimization of a truss-stiffened shell structure and a possibility to combine different types of finite elements within a single design element. The fourth one demonstrates the use of several design elements for a truss-stiffened shell.

Although the finite elements used in this work are non-linear, they may also be used as linear elements. The first three examples are solved by using the linear analysis option. The fourth example is solved by using both the linear and the non-linear option. The optimization process is implemented as shown in Figure 8. For the built-in optimization algorithm of the optimizer the gradient-based approximation method described in [15,14] is employed.

5.1 A pressure vessel strip

Consider a long cylindrical pressure vessel loaded by an inner pressure. It is well known that in cylindrical vessel the bending stresses vanish. This fact is considered in estimating the performance of the proposed approach as well as the accuracy of the employed elements. Starting from a non-circular initial shape a bending-stresses-minimizing shape optimization is performed. The difference between the optimized design and the theoretical (circular) shape will give some indication on the performance of the proposed approach. Only one quarter of a thin strip of the vessel is considered and a straight strip is taken as the starting design (see Figure 9).

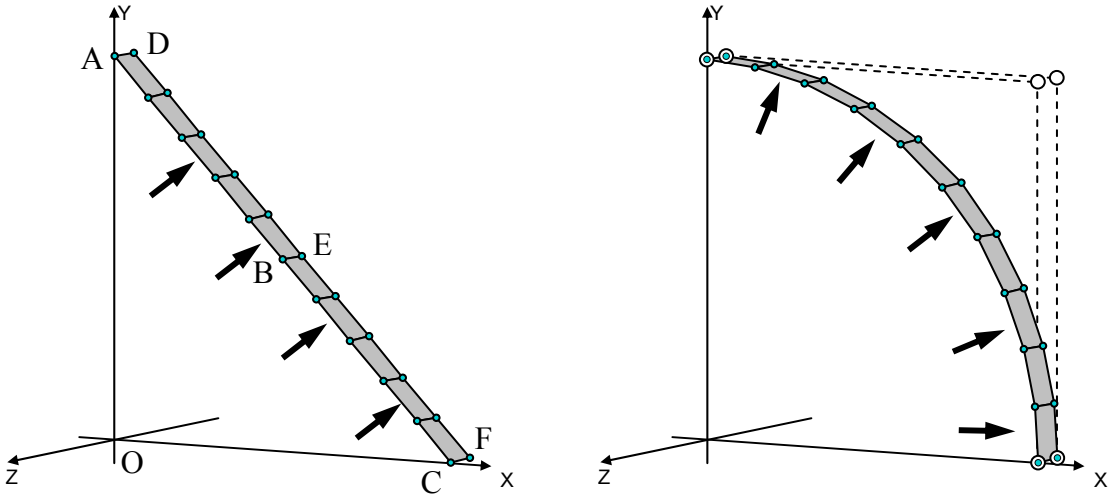

Figure 9. The starting and the final shape of the strip; (design dependent) pressure load

The data of the structure are as follows. The distances are: $\overline{OA} = \overline{OC} = 1000\,\text{mm}$, $\overline{AD} = \overline{BE} = \overline{CF} = 100\,\text{mm}$, and the thickness of the shells is $t = 10\,\text{mm}$. The material is linear

elastic with Young's modulus $E = 210000\,\text{MPa}$ and Poisson's ration is $\nu = 0.3$. The structure is loaded by inner pressure of $p = 1\,\text{MPa}$.

To parametrize the shape of the structure, only one design element with $3 \times 2 \times 1 = 6$ control points is needed, defined as given in Table I.

Table I. Control point definitions

Control point	X	Y	Z	Weight
A	0	1000	0	1
B	$500 + 1000b_1$	$500 + 1000b_2$	0	b_3
C	1000	0	0	1
D	0	1000	-100	1
E	$500 + 1000b_1$	$500 + 1000b_2$	-100	b_3
F	1000	0	-100	1

Thus, three design variables are introduced. Two of them related to the position of intermediate control points and one to their weights. From Table I one can conclude that the starting design is given by $b_1 = b_2 = 0, b_3 = 1$ and that the expected final design is $b_1 = b_2 = \frac{1}{2}, b_3 = \frac{\sqrt{2}}{2}$, which corresponds exactly to a quarter of a circle.

The formulation of the optimization problem is based on the assumption that the minimization of bending stresses may be conveniently achieved by minimizing the strain energy C of the structure. Thus, the objective function (to be minimized) is defined as

$$f_0 = C \tag{20}$$

There are no further mechanical constraints related to the problem, so the number of behavior constraints is zero. Regarding the limits of the design variables, however, it should be noted that the weight of a control point must be a positive quantity. Thus, a positive lower limit of b_3 is here defined by $b_3 \geq 0.1$.

Table II. Final values of the design variables and the corresponding errors in [%]

Variable	Initial	Optimal			Analytical
		10 elements	20 elements	30 elements	
b_1	0	0.497708 (0.46)	0.498098 (0.38)	0.498150 (0.37)	0.5
b_2	0	0.497708 (0.46)	0.498098 (0.38)	0.498150 (0.37)	0.5
b_3	1	0.711677 (0.65)	0.710933 (0.54)	0.710843 (0.53)	0.707107
Distance $\overline{OB}$	707.107	999.758 (0.0242))	999.809 (0.0191)	999.818 (0.0182)	1000

In order to estimate the accuracy of the elements, the problem is solved using three different

meshes: 10, 20 and 30 finite elements. The results are summarized in Table II. It can be seen that the errors computed with respect to the analytical solution decrease with the increasing number of elements. The error magnitudes, however, are in any case quite small. This becomes especially obvious when observing visually the shapes of the three optimal solutions. None of them can be distinguished from the exact circular shape. The radii of all optimized strips differ from the analytical value by less than 0.025%.

It can be concluded that the proposed approach gives very satisfactory results. It also seems that (at least for this example) the 4-node finite element performs quite well. The accuracy of all three meshes is satisfactory.

5.2 A free-form variable-thickness shell structure

The second example is partially taken from [28]. The ground plan of the structure is shown in Figure 10. The four corner points of the structure have hinged supports. The material properties are $E = 30000\ \mathrm{N/mm^2}$ and $\nu = 0.3$. The structure is loaded by a uniform snow load of $w = 5\ \mathrm{kN/m^2}$.

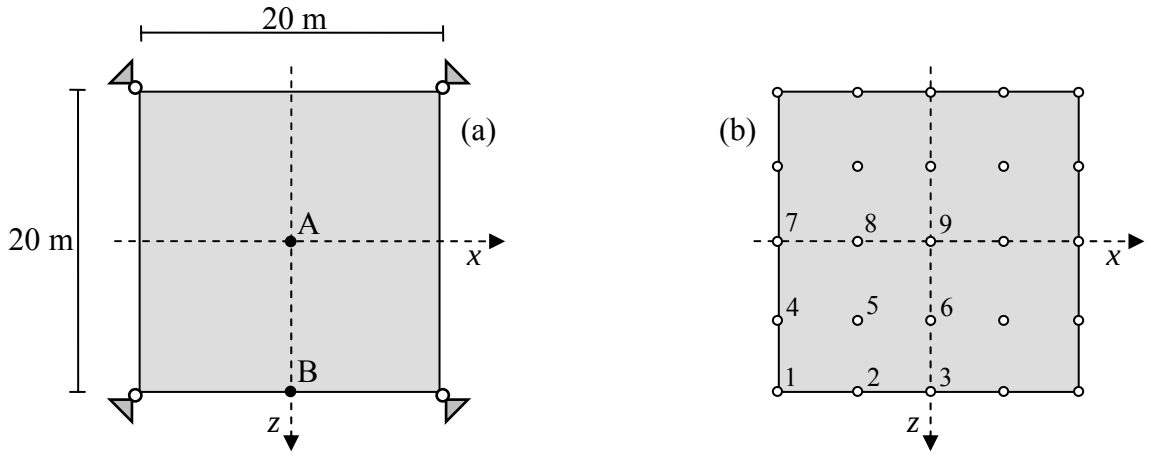

Figure 10. Ground plan of the structure and the positions of the control points

The objective is to optimize the shape and the thickness distribution of the shell by minimizing its relative strain energy

$$c = C/C^{Ini} \tag{21}$$

where the symbol C^{Ini} denotes the strain energy of the shell at the initial (starting) design. Three different optimization problems will be considered, distinguished by the constraints imposed on the vertical positions y_A and y_B of points A and B respectively (see Figure 10a):

Case A. $y_A \geq 8\ \mathrm{m}$

Case B. $y_A \geq 8\ \mathrm{m}$ and $y_B = 8\ \mathrm{m}$

Case C. $8\ \mathrm{m} \leq y_A \leq 9\ \mathrm{m}$ and $y_B = 8\ \mathrm{m}$

In addition to the above constraints the structural volume is constrained to be equal to $V = 60\,\mathrm{m}^3$ in all cases.

A single design element with $5 \times 5 \times 1 = 25$ control points is used to parametrize the structure, Figure 10b. The design variables are related to the control point positions (variable shape) and control point values (variable thickness). The design dependency of the control points 1 through 9 (Figure 10b) is given in Table III. For other control points the design dependency can be easily found by taking into account the symmetry of the structure. It should be noted that the constant factors in the expressions are selected so that the order of magnitude of all design variables is close to 1.

Table III. Design dependency of the control points

Control point	X	Y	Z	Value
1	-10000	0	10000	$150\,b_9$
2	$-5000b_1$	$8000b_4$	10000	$150\,b_{10}$
3	0	$8000b_5$	10000	$150\,b_{12}$
4	-10000	$8000b_4$	$5000b_1$	$150\,b_{10}$
5	$-5000b_2$	$8000b_6$	$5000b_2$	$150\,b_{11}$
6	0	$8000b_7$	$5000b_3$	$150\,b_{13}$
7	-10000	$8000b_5$	0	$150\,b_{12}$
8	$-5000b_3$	$8000b_7$	0	$150\,b_{13}$
9	0	$8000b_8$	0	$150\,b_{14}$

Table III shows that there are 8 design variables (1-8) related to the shape, and 6 design variables (9-14) related to the thickness of the shell. In order to prevent unacceptable designs, the upper and the lower bounds of the design variables were selected as given in Table IV. This table also shows the initial values of the design variables that correspond to a flat quadratic shell with constant thickness of $t = 150\,\mathrm{mm}$.

Table IV. Design variable values and relative strain energies

Variable	Lower	Upper	Initial	Optimal A	Optimal B	Optimal C
1	0	1.9	1	0.72549	1.54440	0.0000
2	0	1.9	1	1.63736	0.90135	0.29797
3	0	1.9	1	0.19567	0.80382	1.20836
4	0	4	0	0.63336	0.22387	1.17240
5	0	4	0	0.85788	2.36815	1.10313
6	0	4	0	0.50935	0.00000	0.38237
7	0	4	0	2.32411	2.92379	1.92528
8	0	4	0	0.28598	0.16219	0.40860
9	0.1	4	1	3.82926	4.00000	1.38361
10	0.1	4	1	0.1	0.24125	1.13367
11	0.1	4	1	0.10120	0.17162	0.1
12	0.1	4	1	0.1	0.30133	0.1
13	0.1	4	1	0.11704	0.11988	0.41254
14	0.1	4	1	0.17143	0.10183	0.45508
c	-	-	-	0.24936E-3	0.26322E-3	0.35349E-3

All three cases were solved without problems with the employed optimizer. The final shapes are shown in Figure 11.

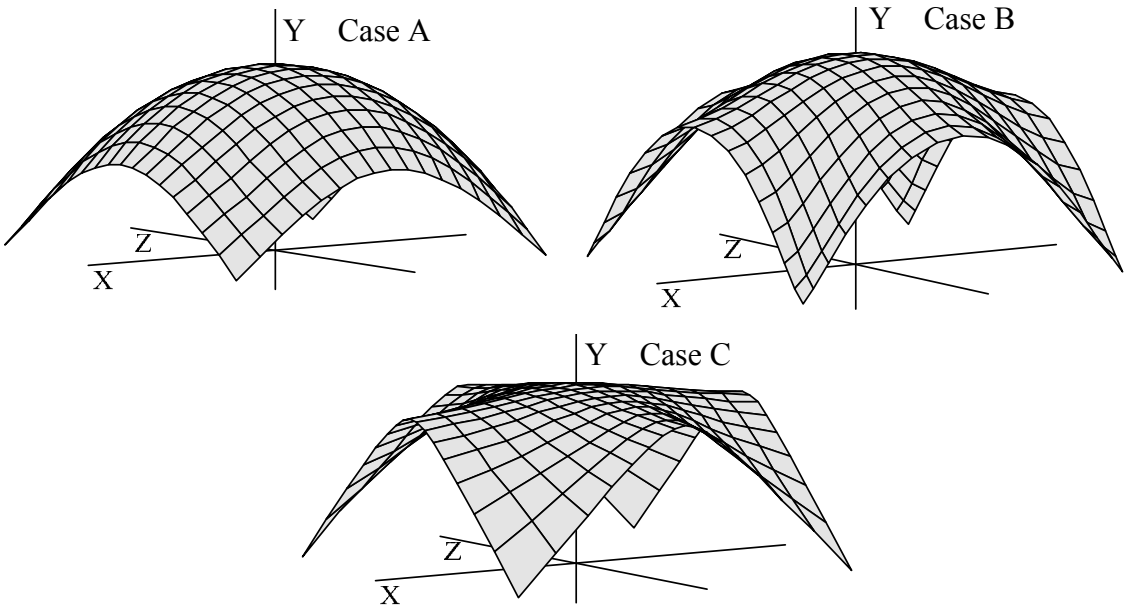

Figure 11. Optimal shell shapes for cases A, B and C

Since A is the least and C the most constrained case, one would expect that the strain energy of the optimized structure is also the smallest for case A and the largest for case C. As can be seen from Table IV, numerical results confirm such expectation. Compared to case A, the strain energy has increased by 5.6% in case B and by 41.8% in case C.

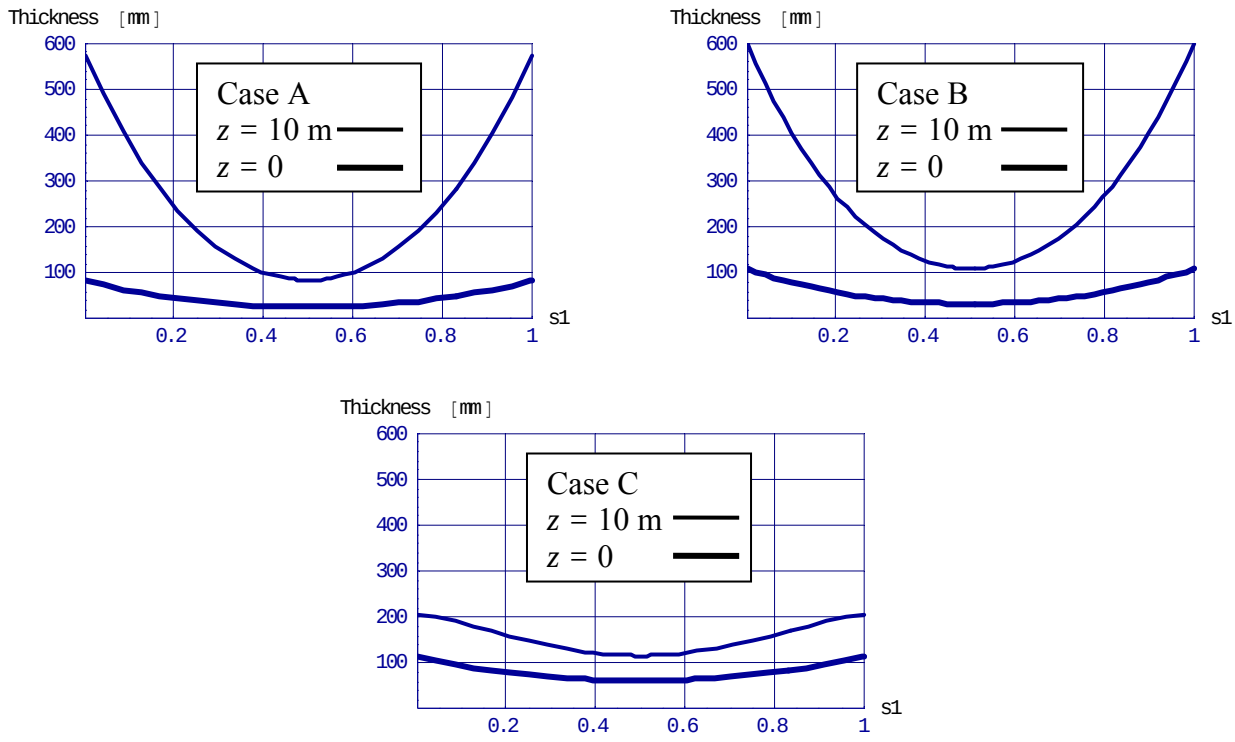

Figure 12. Thickness distribution of optimal shapes at cross-sections at $z = 0$ and $z = 10$ m

Figure 12 illustrates the thickness distribution of the shell. As can be seen in cases A and B the thickness variation is quite large, while in case C the thickness variation is rather moderate. This is probably is due to the fact that design C exhibits rather large areas with moderate curvature. Except in the middle, the edges are almost straight in case C. It should also be noted that in case B one thickness variable reached its upper limit. By relaxing this constraint, the thickness variation would probably increase even more.

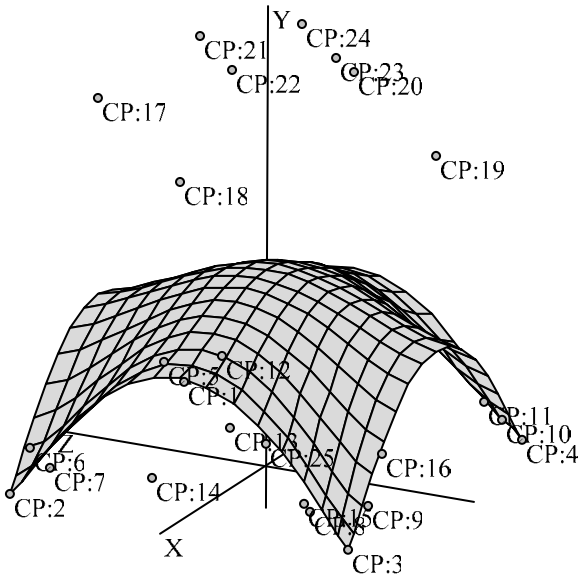

Figure 13. Control point positions at the final design in case B

Finally, to illustrate the movement of the control points, Figure 13 shows their positions for

the final design in case B. Note that initially all control points were positioned in the $y = 0$ plane.

5.3 A truss-stiffened free-form shell structure

As a third example an asymmetric structure is considered. The shell is pin-jointed to the upper layer of a double-layered truss structure (see Figure 14). The thickness of the shell is constant and equal to 5 mm. All truss elements are pipes with the outer radius equal to 3 cm and wall thickness equal to 3 mm. The material properties are $E = 210000\,\text{MPa}$, $\nu = 0.3$ and $\rho = 7800\,\text{kg/m}^3$. Along both longer edges the structure is supported by hinges. The loading consists of self-weight and a uniform snow load of $w = 1.5\,\text{kN/m}^2$.

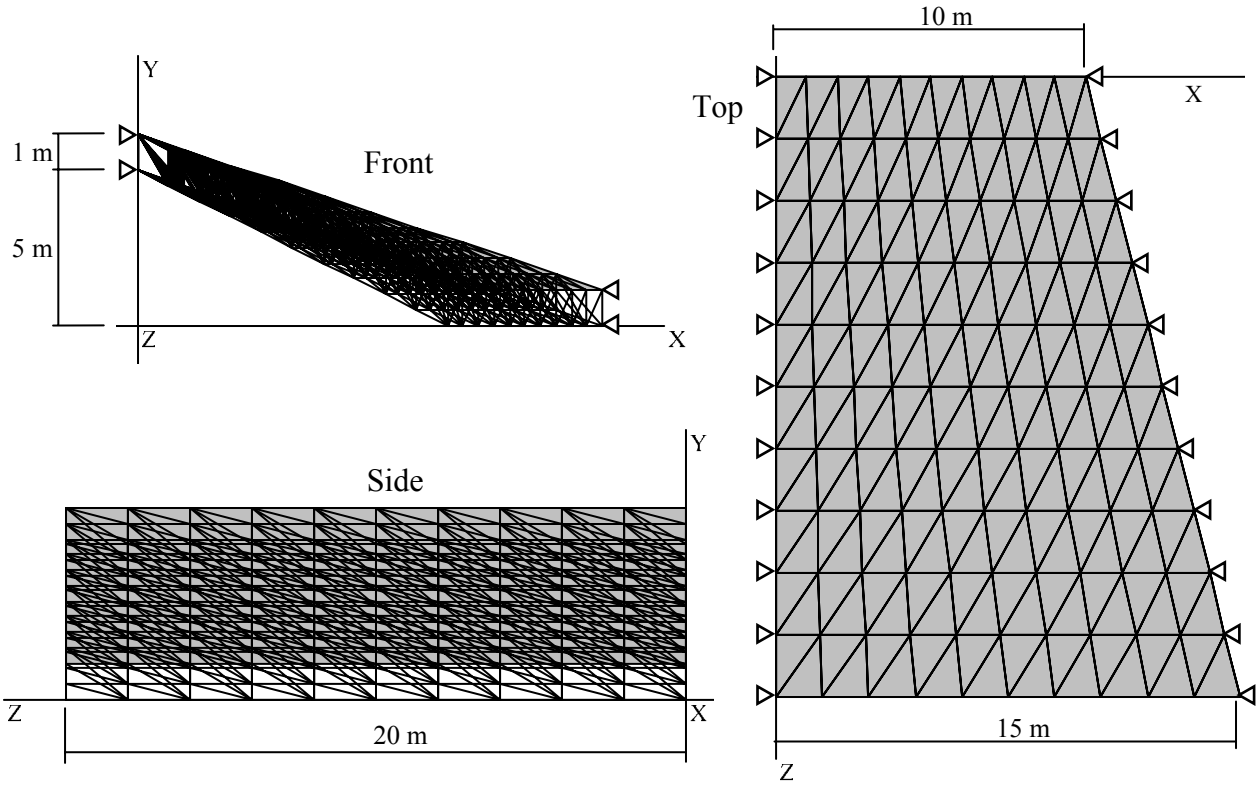

Figure 14. Front, side and top view of the structure – initial design

The objective is to optimize the shape of the structure by minimizing c_s and c_t where c_s and c_t denote the relative strain energies of the shell and the truss, respectively. The constraints are related to structural geometry and to the buckling of truss elements. The geometric constraints are defined as $v_t \le 1$, $5\,\text{m} \le y_0 \le 5.5\,\text{m}$ and $5\,\text{m} \le y_{20} \le 6\,\text{m}$. The symbol v_t denotes the relative volume of the truss (actual volume divided by its value at the initial design), while y_0 and y_{20} denote the y coordinate of the apex of the lower truss layer at $z = 0\,\text{m}$ and $z = 20\,\text{m}$, respectively. For each truss element its stress is constrained by $\sigma_i \ge \sigma_{iE}/2$ where σ_{iE} denotes the Euler buckling stress of the *i-th* element. Two different optimization problems will be considered, distinguished by

the definition of the objective function f_0:

Case A. $f_0 = c_s$

Case B. $f_0 = c_s + c_t$

Thus in case A only the strain energy of the shell is minimized while in case B the objective function is the sum of relative strain energies of the shell and truss.

A single design element with $3 \times 4 \times 2 = 24$ control points is used to parametrize the structure (see Figure 15). The design variables are related to the control point positions, as given in Table V. By these definitions the order of magnitude of the design variables is close to unity and the minimal vertical distance between two vertical points is 0.15 m.

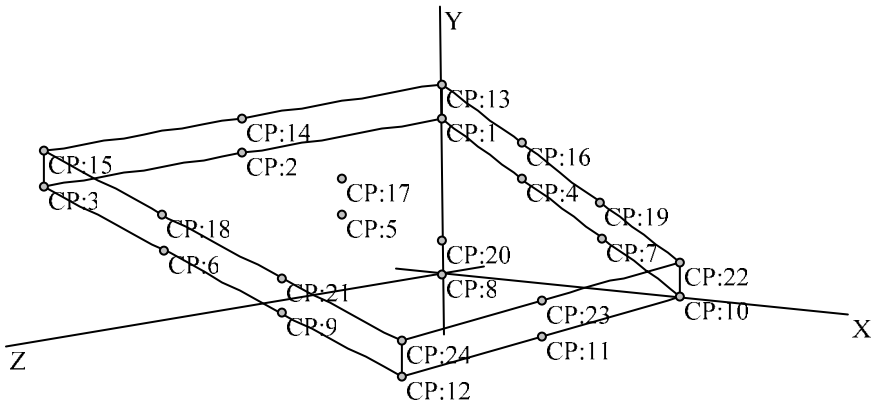

Figure 15. Design element and control point positions – initial design

Table V. Design dependency of the control point positions

Control point	Y	Control point	Y
4	$3.33 + 5b_1$	16	$3.48 + 5b_1 + b_{10}$
5	$3.33 + 5b_2$	17	$3.48 + 5b_2 + b_{11}$
6	$3.33 + 5b_3$	18	$3.48 + 5b_3 + b_{12}$
7	$1.66 + 5b_4$	19	$3.48 + 5b_4 + b_{13}$
8	$1.66 + 5b_5$	20	$3.48 + 5b_5 + b_{14}$
9	$1.66 + 5b_6$	21	$3.48 + 5b_6 + b_{15}$
13	$5.15 + b_7$	22	$0.15 + b_{16}$
14	$5.15 + b_8$	23	$0.15 + b_{17}$
15	$5.15 + b_9$	24	$0.15 + b_{18}$

Thus, 18 design variables are introduced. Their lower and upper limit values are given in Table VI. The optimization process started in both cases from the initial design given in the same table. The process was smooth and stable with an almost monotonic objective function history.

The final results are compared in Tables VI and VII. Although the difference seems not to be so dramatic when looking at the final shapes superficially (see Figures 16 and 17), it can be seen that from the numerical point of view both results are quite different. Also, a closer look at the shape of the truss reveals that shape B is much more elegant and more intuitive.

Table VI. Design variable values

Variable	Lower	Upper	Initial	Optimal A	Optimal B
1	0	2	0	0.76967	0.57851
2	0	2	0	1.63425	2
3	0	2	0	0.77647	0.73827
4	0	2	0	0.32051	0.76656
5	0	2	0	0.24360	1.92769
6	0	2	0	0.83374	0.92288
7	0	1	1	0	0
8	0	1	1	0.40629	0
9	0	1	1	0	0
10	0	1	1	1	0.95028
11	0	1	1	0.92404	0.84638
12	0	1	1	1	1
13	0	1	1	0	0
14	0	1	1	0	0.15654
15	0	1	1	0.33434	0.49471
16	0	1	1	1	0.39225
17	0	1	1	1	0.98491
18	0	1	1	1	0.36351

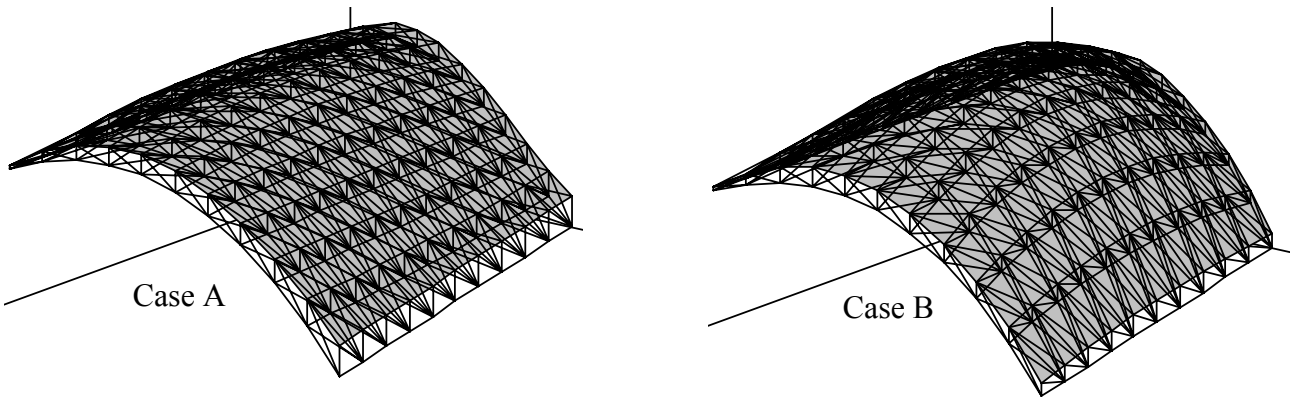

Figure 16. Optimal design of cases A and B

Table VII shows that the strain energy of the shell is slightly larger in case B, but the strain energy of the truss is significantly lower. Thus, in this particular case it seems that a more efficient structure was obtained by taking into account both strain energies. For a general case, however, this is difficult to predict. The reason is that the problem of minimizing both strain energies is actually a multiobjective optimization problem whose solutions are termed the Pareto set. In this case a

common procedure was employed to transform the multiobjective problem into its scalar substitute by summing up both strain energies, multiplied by such weights that their initial values were equal to 1. In this way only a single Pareto optimal point was obtained. In order to search through the whole Pareto set, special strategies need to be employed (see e.g. [23]). This topic, however, is beyond the scope of this paper.

Table VII. Relative strain energies

	Initial	Optimal A	Optimal B
c_s	1	0.20524	0.22380
c_t	1	0.26835	0.00794
$c_s + c_t$	2	0.47359	0.23175

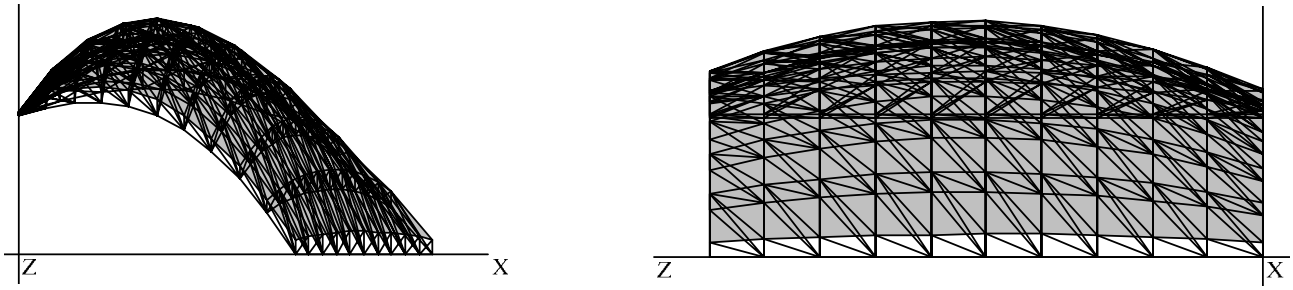

Figure 17. Optimal design of case B - front and side view

5.4 A truss-stiffened free-form shell structure modeled with several design elements

In the fourth example the structure consists of a shell supported by a slender truss stiffener in the middle of its span (see Figure 18). The thickness of the shell is constant and equal to 1 cm. All truss elements are pipes with the outer radius equal to 2 cm and the wall thickness equal to 2 mm. The material properties are $E = 210000\,\text{MPa}$, $\nu = 0.3$ and $\rho = 7800\,\text{kg/m}^3$. Along both shorter edges of the shell as well as on both ends of the truss the structure is hingly supported. The structure is loaded by its own weight and a uniform snow load of $w = 1.5\,\text{kN/m}^2$.

The objective is to optimize the shape of the structure by minimizing the strain energies of the truss and the shell. As mentioned in the above example, this is again a multiobjective problem. Its scalar substitute is obtained by defining a single objective function as a sum $c = c_s + c_t$ of relative strain energies of the shell and the truss, respectively. The constraints are related to the relative volume v_t of the truss, which should not increase, and to the vertical coordinate y_A of point A of the shell, which must be between 1 and 2 m. Thus one has $v_t \le 1$ and $1\,\text{m} \le y_A \le 2\,\text{m}$.

Three design elements are employed to parametrize the shape of the structure. The first design

element with $3\times2\times2=12$ control points is used for the truss and the shell elements attached to its upper layer (see Figure 19). The other two design elements with $3\times3\times1=9$ control points are used for the left and right wing of the shell, respectively. Only positional continuity is required on the common boundaries of the design elements. The design variables are related to the control point positions as given in Table VIII. The vertical coordinates of the control points, not listed in the table, can be found by symmetry.

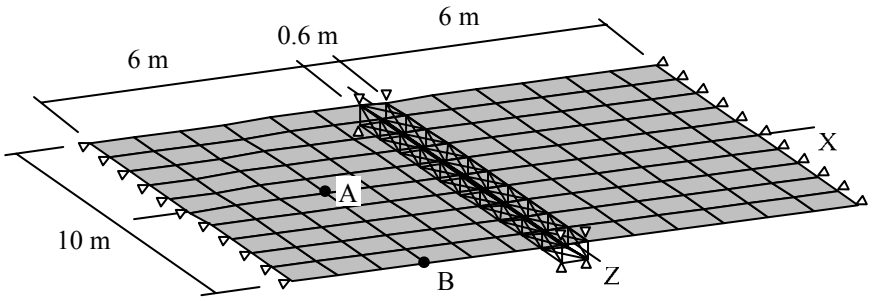

Figure 18. Shell supported by a slender truss

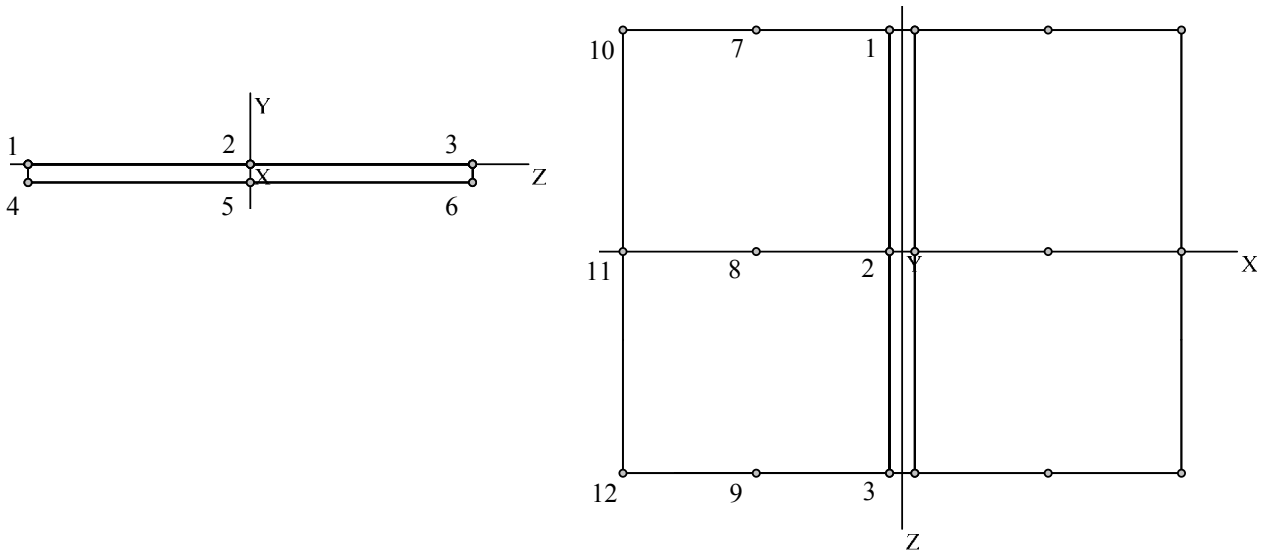

Figure 19. Design elements and their control points

Table VIII. Vertical coordinates of the control points and their design dependency

Control point	Y	Control point	Y
1	0	7	$5b_5$
2	$5b_1$	8	$5b_4$
3	0	9	$5b_5$
4	$0.15b_3-0.4$	10	0
5	$5b_1-0.4(1+b_2)$	11	0
6	$0.15b_3-0.4$	12	0

For the optimization process, both linear and non-linear options for the structural model are used. Although the displacements are assumed to be small, it might be interesting to see the differences in the obtained results.

5.4.1 Linear structural model

The optimization process was started from the initial design shown in Figure 18. The employed gradient-based optimizer converged to design A shown in Figure 20. Since there are not many constraints, the truss was reshaped manually to form an arch. For this purpose, the first design variable b_1 was reset to its upper limit and the optimization process was restarted. The structure was reshaped completely and converged to design B shown in Figure 21. The objective function of design B is lower than that of design A. This means that the first result was surely not the global solution.

By observing the result B one gets the impression that the result might be further improved by lowering the vertical position of point B (see Figure 18). Therefore, the value of the design variable b_5 was reduced. After restarting the optimization process, the structure was reshaped again and converged to design C, shown in Figure 22. This is the result with the lowest objective function value. Since further local optima could not be found, it can be concluded with reasonable probability that for the considered problem there are three local optima, design C being the best. Thus, design C is probably also the global solution of the problem. The design variable values and the relative strain energies for all solutions are listed in Tables IX and X.

Table IX. Design variable values

Variable	Lower	Upper	Initial	Optimal A	Optimal B	Optimal C
1	0	2	0	0	0.77214	0.119625
2	0	2	0	0	0	0.33406
3	0	2	0	2	2	2
4	0	2	0	0.95284	0.29530	1.12396
5	0	2	0	0.64716	0.73070	0.41624

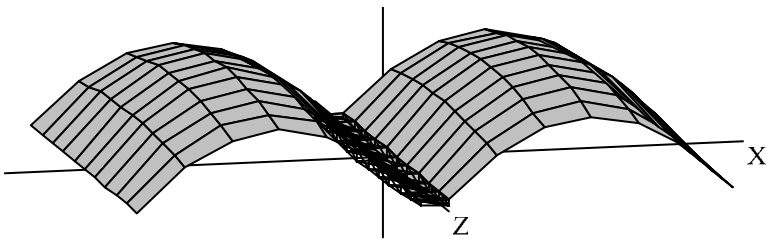

Figure 20. Optimal design A (L model)

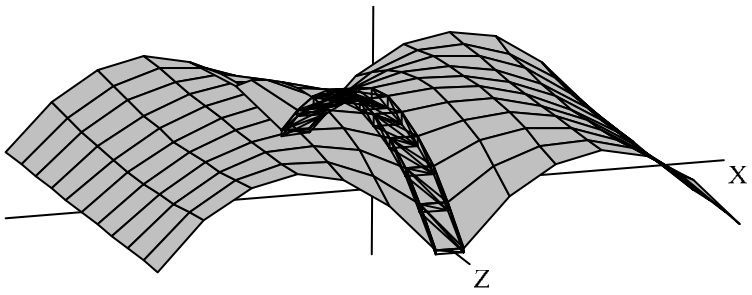

Figure 21. Optimal design B (L model)

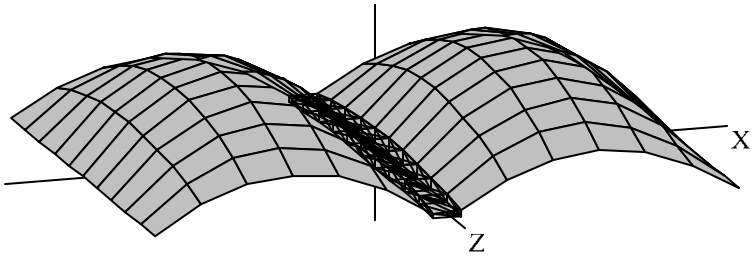

Figure 22. Optimal design C (L model)

Table X. Relative strain energies

	Initial	Optimal A	Optimal B	Optimal C
c_s	1	0.25667E-3	0.06570E-3	0.15682E-3
c_t	1	0.27203E-3	0.43407E-3	0.18037E-3
$c = c_s + c_t$	2	0.52870E-3	0.49977E-3	0.33719E-3

This example shows that also rather small design problems with only a few design variables might well have several local optima being quite diverse in their shape. Care should therefore be taken when formulating and solving such optimization problems. In any case, it seems to be a good idea to run the optimization process from several starting points that correspond approximately to some designs that are expected to be efficient by intuition. The other possibility would be to use one of the evolutionary optimizers. This would substantially increase the probability to find the global optimum.

5.4.2 Non-linear structural model

Starting from the same initial design as with the linear model, the solution process converged quickly to design D, shown in Figure 23. Note that the obtained solution is quite similar to design B obtained with the linear model. The main difference is a somewhat increased curvature of the structure.

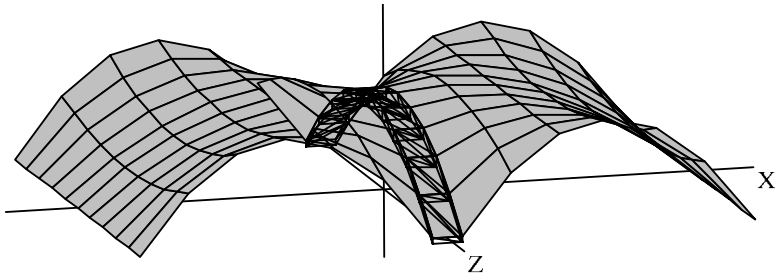

Figure 23. Optimal design D (NL model)

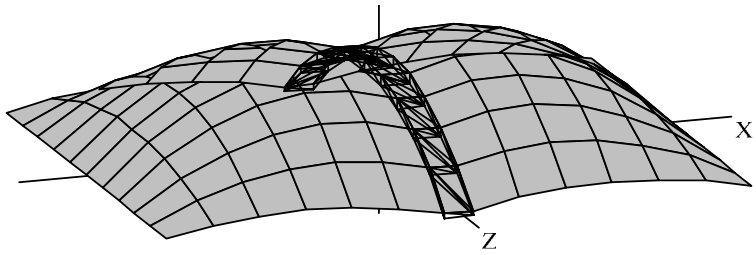

Figure 24. Optimal design E (NL model)

For the same reasons as already discussed with the linear model, the vertical position of point B was lowered in order to restart the optimization process and to search for another optimum solution. The structure was reshaped and the optimization process converged to design E, shown in Figure 24. Note that this result does not show much similarity with the designs obtained by using the linear model.

Table XI. Design variable values

Variable	Lower	Upper	Initial	Optimal D	Optimal E
1	0	2	0	0.77214	0.77214
2	0	2	0	0	0
3	0	2	0	2	2
4	0	2	0	0.11925	1.08156
5	0	2	0	0.88642	0.13241

Table XII. Relative strain energies

	Initial	Optimal D	Optimal E
c_s	1	5.49397E-3	5.82268E-3
c_t	1	0.65988E-3	0.62373E-3
$c = c_s + c_t$	2	6.15385E-3	6.44641E-3

The values of the design variables, corresponding to designs D and E, are given in Table XI. The corresponding strain energies are listed in Table XII. It can be seen that design D exhibits a

lower objective function value. Thus, design E is obviously only a local optimum.

Finally, it might be interesting to compare all of the obtained results with respect to the structural strain energies. For this purpose all designs were analyzed using the non-linear analysis option and the results are summarized in Table XIII. It is obvious that designs B, D and E are all quite good compared to C, and especially to A. It is interesting to note that here design C looks worse than B which seems to be in contrast with the data given in Table X. This, however, is only a consequence of the employed weighting factor values used to define the relative strain energies of the structure.

Table XIII. Strain energies calculated using the NL analysis option

	Optimal A	Optimal B	Optimal C	Optimal D	Optimal E
C_s	52984	10947	26523	10680	11319
C_t	341	566	233	571	539
$C = C_s + C_t$	53325	11513	26756	11251	11858

CONCLUSIONS

The proposed procedure offers a unified approach to shape optimization of variable thickness shell structures with or without truss stiffeners. A body-like design element enables consistent shape variations of both the shell and the truss part of the structure. The smoothly varying thickness of the shell is introduced in a simple manner by a scalar field defined over the design element. The presented numerical examples indicate that the proposed approach performs quite well, although there are several aspects requiring careful consideration.

Firstly, for truss-stiffened shells the design problem often becomes a multiobjective one. On one hand, transforming the multiobjective problem into a conventional one is a very challenging task, since the results may depend significantly, for example, on the weighting factors used. On the other hand, ‘keeping’ the problem multiobjective and performing a systematic search through the Pareto set requires numerical implementation of adequate strategies and substantial increase of computational effort.

Secondly, there is a question regarding the use of linear or non-linear structural analysis. As shown in the last example, different models may lead to quite diverse results although the actual displacements of the structure are quite small. This might be a consequence of the fact that slight shape changes of the feasible domain of the problem may easily shift the optimal point substantially if the feasible domain is locally flat. In such a situation a slight shape change of the domain may also cause a gradient-based optimizer to converge to different local solutions.

REFERENCES

[1] Ansola R, Canales J, Tarrago JA, Rasmussen J. An integrated approach for shape and topology optimization of shell structures. . Computers & Structures 2002; 80: 449-458.

[2] Ansola R, Canales J, Tarrago JA, Rasmussen J. On simultaneous shape and material layout optimization of shell structures. Structural and Multidisciplinary Optimization 2002; 24, 175–184.

[3] Bathe KJ, Dvorkin E, A four-node plate bending element based on Reissner-Mindlin plate theory and a mixed interpolation, Int. J. Numer. Methods Engng. 1985; 21: 367-383.

[4] Belblidia F, Bulman S. A hybrid topology optimization algorithm for static and vibrating shell structures. International Journal for Numerical Methods in Engineering 2002; 54: 835–852.

[5] Bletzinger K-U. Structural optimization and form finding of light weight structures. Proceedings of the European Conference on Computational Mechanics 1999 (ed. Wunderlich W). Muenchen, Germany.

[6] Borri C, Mirto F. Numerical form finding for multiple R.C. thin shells with arbitrarily irregular ground plan. Computational Methods for Shell and Spatial Structures IASS-IACM 2000, Papadrakakis M et al (Eds.), Athens, Greece.

[7] Brank B, Ibrahimbegović A. On the relation between different parametrizations of finite rotations for shells, Engineering Computations 2001; 18: 950-973.

[8] Brank B, Perić D, Damjanić FB. On implementation of a nonlinear four node shell finite element for thin multilayered elastic shells. Computational Mechanics 1995; 16: 341-359.

[9] Camprubi N, Bischoff M, Bletzinger KU. On the significance of locking on shape optimization of shells. Proceedings of Second MIT Conference on Computational Fluid and Solid Mechanics, Bathe KJ (ed.), Elsevier, 2003.

[10] Farin G. Curves and Surfaces for Computer Aided Geometric Design (2nd edn). Academic Press: New York, 1993.

[11] Gates AA, Accorsi ML. Automatic shape optimization of three-dimensional shell structures with large shape changes. Computers & Structures 1993; 49: 167-178.

[12] Ibrahimbegović A, Knopf-Lenoir C, Kučerova A, Villon P., Optimal design and optimal control of structures undergoing finite rotations and elastic deformations, Int. J. Numer. Methods Engng. 2004; 61: 2428-2460.

[13] Imam MH. Shape optimization of umbrella-shaped concrete shells subjected to self-weight as the dominant load. Computers & Structures 1998; 69: 513-524.

[14] Kegl M, Butinar BJ, Kegl B. An efficient gradient-based optimization algorithm for mechanical systems. Communications in Numerical Methods in Engineering 2002; 18: 363-371.

[15] Kegl M, Oblak MM. Optimization of mechanical systems: on non-linear first-order approximation with an additive convex term. Communications in Numerical Methods in

Engineering 1997; 13: 13-20.

[16] Kegl M. Shape optimal design of structures: an efficient shape representation concept. International Journal for Numerical Methods in Engineering 2000; 49: 1571-1588.

[17] Kim NH, Choi KK, Chen JS, Botkin ME. Meshfree analysis and design sensitivity analysis for shell structures. International Journal for Numerical Methods in Engineering 2002; 53: 2087-2116.

[18] Korelc J, Automatic generation of numerical codes with introduction to AceGen 4.0 symbolic code generator, University of Ljubljana, Faculty of Civil and Geodetic Engineering, available from www.fgg.uni-lj.si/Symech/; 2005.

[19] Lagaros ND, Fragiadakis M, Papadrakakis M. Optimum design of shell structures with stiffening beams. AIAA Journal 2004; 42: 175-184.

[20] Lee SJ, Hinton E. Dangers inherited in shells optimized with linear assumptions. Computers & Structures 2000; 78: 473-486.

[21] Lindby T, Santos JLT. Shape optimization of three-dimensional shell structures with the shape parametrization of a CAD system. Structural Optimization 1999; 18: 126-133.

[22] Maute K, Ramm E. Adaptive topology optimization of shell structures. AIAA journal 1997; 35: 1767-1773.

[23] Messac A, Ismail-Yahaya A, Mattson CA, The normalized normal constraint method for generating the Pareto frontier, Structural and Multidisciplinary Optimization. 2003; 25: 86-98.

[24] Ohsaki M, Nakamura T, Isshiki Y. Shape-size optimization of plane trusses with designer's preference. Journal of Structural Engineering-ASCE 1998; 124: 1323-1330.

[25] Ohsaki M, Ogawa T, Tateishi R. Shape optimization of curves and surfaces considering fairness metrics and elastic stiffness. Structural and Multidisciplinary Optimization 2003; 24, 449–456.

[26] Pourazady M, Fu Z. An integrated approach to structural shape optimization. Computers & Structures 1996; 60: 279-289.

[27] Ramm E, Kemmler R, Schwarz S, Formfinding and Optimization of Shell Structures. Proceedings of the Fourth International Colloquium on Computation of Shell & Spatial Structures, Papadrakakis M et al. (eds.) 2000.

[28] Reitinger R, Ramm E. Buckling and imperfection sensitivity in the optimization of shell structures. Thin-Walled Structures 1995; 23: 159-177.

[29] Ryu JS, Haririan M, Wu CC, Arora JS, Structural design sensitivity analysis of nonlinear response. Computers & Structures 1985; 21: 245-255.

[30] Simo JC, Fox DD, Rifai SM, On a stress resultant geometrically exact shell model. Part III: Computational aspects of the nonlinear theory, Comput. Methods Appl. Mech. Engrg. 1990; 79: 21-